Multiexciton Generation in Seeded Nanorods

Hagai Eshet,*,[†] Roi Baer,*,[‡] Daniel Neuhauser,*,[¶] and Eran Rabani*,[†]
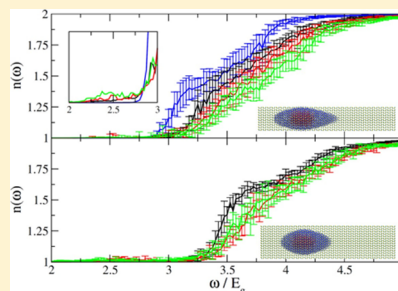
[†]School of Chemistry, The Sackler Faculty of Exact Sciences, Tel Aviv University, Tel Aviv 69978, Israel

[‡]Fritz Haber Center for Molecular Dynamics, Institute of Chemistry, The Hebrew University of Jerusalem, Jerusalem 91904, Israel

[¶]Department of Chemistry, University of California at Los Angeles, Los Angeles, California 90095, United States

ABSTRACT: The stochastic formulation of multiexciton generation (MEG) rates is extended to provide access to MEG efficiencies in nanostructures containing thousands of atoms. The formalism is applied to a series of CdSe/CdS seeded nanorod heterostructures with different core and shell dimensions. At energies above $3E_g$ (where E_g is the band gap), the MEG yield increases with decreasing core size, as expected for spherical nanocrystals. Surprisingly, this behavior is reversed for energies below this value, and is explained by the dependence of the density of states near the valence band edge, which increases with the core diameter. Our predictions indicate that the onset of MEG can be shifted to lower energies by manipulating the density of states in complex nanostructure geometries.

Multiexciton generation yield in CdSe/CdS seeded nanorods.

SECTION: Physical Processes in Nanomaterials and Nanostructures

Multiexciton generation by which more than a single electron–hole pair is generated from a single photon upon optical excitation is a promising direction to collect "hot" carriers, potentially increasing photovoltaic power conversion efficiencies in solar cells to above 45%.[1,2] It is common to define an onset photon energy E_{on} beyond which multiexciton generation (MEG) efficiencies are noticeable. One of the necessary conditions for MEG to be of technological use is that E_{on} be close to the lower bound of twice the quasiparticle band gap ($2E_g$).[1] In bulk semiconductors, $E_{on}/E_g > 5$, and thus, MEG is not useful for photovoltaic applications. This large ratio is a consequence of energy and momentum conservation constraints, which severely limit the number of multiexciton states that can be formed, coupled with the existence of very rapid nonradiative relaxation pathways.[3,4] Confined semiconductor nanocrystals (NCs), on the other hand, offer improved MEG efficiencies,[5,6] with an onset energy below $E_{on} < 3E_g$.[7–17] This result was rationalized by several different theoretical treatments.[18–31] Perhaps the most intuitively appealing picture of MEG in NCs is that of impact ionization.[18,19,21,29] Using this framework and a unified Green function approach to MEG, it was shown that size scaling of the band gap, Coulomb couplings, and density of states (DOS) lead to an overall increase in MEG rates and efficiencies with decreasing NC size when the photon energy is scaled by E_g.[32]

Several different approaches have been proposed recently to lower the onset energy ratio E_{on}/E_g. Gabor et al.[33] used internal fields to decrease E_{on}/E_g in carbon nanotube photodiodes, a result that was rationalized by field-induced acceleration of the charge carriers.[34] Sandberg et al.[35] studied the role of shape on MEG efficiency and argued for a 60% increase in MEG yields in semiconductor nanorods (NRs) compared to spherical NCs.

The effect of NR diameter and length on MEG rates was analyzed by considering the scaling of the density of trion states (DOTS) and the Coulomb couplings.[36] Both show distinct scaling from spherical NCs, leading to a surprising result where the MEG rates, which are given by the product of the two, were roughly independent of the NR length.[36] This prediction was recently verified by experiments.[37,38]

Two additional handles can be used to control the onset energy ratio E_{on}/E_g. The first is based on suppressing the competing channel of phonon emission. Klimov and co-workers have recently shown that the MEG onset energy in type-II core–shell NCs can be reduced markedly by partially blocking the nonradiative decay channel.[39] Theoretically, addressing the role of phonon emission in nanostructures is rather challenging.[40,41] The other handle, which forms the crux of our approach, is based on controlling the DOS near the band edge. This allows for reduction of E_{on}/E_g and at the same time an increase of the MEG efficiency. In order to achieve this, we study the MEG efficiency in seeded NR heterostructures[42,43] using a stochastic formulation of the MEG formation rates.[30] We then extend the formalism to calculate the MEG efficiency in a series of seeded NRs with different seed size and different NR diameter. In contrast to the case of spherical NCs, we find that below E_{on}/E_g, the MEG efficiency increases with the seed radius, that is, larger seeds show higher MEG efficiency even when the photon energy is scaled by E_g.

In order to calculate the MEG efficiencies in seeded NRs, we adopt the master equation approach, which assumes that each

exciton generated upon absorption can either decay to the band edge by phonon emission with a rate γ or produce another electron–hole pair with a rate Γ_S. The master equation approach was previously applied to study MEG in spherical NCs and predicts MEG efficiencies similar to those calculated by a direct absorption Green function formalism within the wide band limit.[32] Using the master equation approach, it is straightforward to show that the MEG efficiency is related to the number of excitons generated at steady state, which is given by[21]

$$n_{ex}(\omega) = \sum_S P_S(\omega) \frac{2\Gamma_S + \gamma}{\Gamma_S + \gamma} \qquad (1)$$

where $n_{ex}(\omega)$ represents the number of excitons generated at a photon energy $\hbar\omega$ (the MEG efficiency is simply given by $n_{ex}(\omega) - 1$) and $P_S(\omega)$ is the probability for absorbing the photon and generating an exciton $|S\rangle$ with energy E_S

$$P_S(\omega) = \frac{|\mu_{0S}|^2 \delta(E_S - \hbar\omega)}{\sum_{S'} |\mu_{0S'}|^2 \delta(E_{S'} - \hbar\omega)} \qquad (2)$$

In the above equations, $|S\rangle \equiv |S_{i\sigma}^{a\sigma}\rangle = a_{a\sigma}^\dagger a_{i\sigma}|0\rangle$ is a shorthand notation for a single exciton state obtained by applying the annihilation ($a_{i\sigma}$) and creation ($a_{a\sigma}^\dagger$) operators on the ground state Slater determinant, $|0\rangle$. We use indices i, j, k, ... for occupied (hole) states and a, b, c, ... for unoccupied (electron) states. r, s, t, u, ... are general indices, and $\sigma = \uparrow, \downarrow$ is the spin index. μ_{0S} is the transition dipole from $|0\rangle$ to $|S\rangle$, γ is the phonon emission rate, and Γ_S is the MEG rate from state $|S\rangle$.

It is interesting to note two limits of eq 1: when the MEG rate is much larger than the phonon emission rate ($\Gamma_S \gg \gamma$), MEG becomes highly efficient ($n_{ex}(\omega) \to 2$), and when the phonon emission rate is much larger compared to the MEG rate ($\gamma \gg \Gamma_S$), MEG is suppressed ($n_{ex}(\omega) \to 1$).

The calculation of γ and Γ_S is computationally expensive for large NCs. We take the value of γ from experiments and assume that it is energy-independent.[32] Γ_S is written as as sum of rates of creating positive and negative trions

$$\Gamma_S \equiv \Gamma_{ia} = \Gamma_a^- + \Gamma_i^+ \qquad (3)$$

and a stochastic formula for the negative and positive trion formation rates is adopted[30]

$$\Gamma_a^- = \frac{2\pi}{\hbar} \langle W_a^2 \rangle \rho_T^-(\varepsilon_a)$$

$$\Gamma_i^+ = \frac{2\pi}{\hbar} \langle W_i^2 \rangle \rho_T^+(\varepsilon_i) \qquad (4)$$

where the negative and positive DOTS is given by

$$\rho_T^-(\varepsilon) = \sum_{bcj} \delta(\varepsilon - (\varepsilon_b + \varepsilon_c - \varepsilon_j))$$

$$\rho_T^+(\varepsilon) = \sum_{jkb} \delta(\varepsilon - (\varepsilon_j + \varepsilon_k - \varepsilon_b)) \qquad (5)$$

and the average square Coulomb coupling for electrons and holes is given by

$$\langle W_a^2 \rangle = \frac{\sum_{bcj} W_{a;cbj}^2 \delta(\varepsilon_a - (\varepsilon_b + \varepsilon_c - \varepsilon_j))}{\rho_T^-(\varepsilon_a)}$$

$$\langle W_i^2 \rangle = \frac{\sum_{jkb} W_{i;jkb}^2 \delta(\varepsilon - (\varepsilon_j + \varepsilon_k - \varepsilon_b))}{\rho_T^+(\varepsilon_i)} \qquad (6)$$

In the above equations, the squared Coulomb couplings are given by

$$W_{a;cbj}^2 = 2|V_{acjb} - V_{jcab}|^2 + |V_{jcab}|^2 + |V_{acjb}|^2$$

$$W_{i;jkb}^2 = 2|V_{jibk} - V_{kijb}|^2 + |V_{kijb}|^2 + |V_{jibk}|^2 \qquad (7)$$

where

$$V_{rsut} = \iint d^3r \, d^3r' \, \frac{\psi_r(\mathbf{r})\psi_s(\mathbf{r})\psi_u(\mathbf{r}')\psi_t(\mathbf{r}')}{\epsilon|\mathbf{r} - \mathbf{r}'|} \qquad (8)$$

is the screened Coulomb interactions and $\psi_r(\mathbf{r})$ are the single-particle orbitals (see more details below). We assume a static dielectric screening, ϵ, for the Coulomb matrix elements.

To calculate the MEG efficiency given by eq 1, one requires as input the MEG rates and the transition probabilities for all possible single excitons $|S\rangle \equiv |S_{i\sigma}^{a\sigma}\rangle$. For spherical NCs, these are readily available for moderate excitation energies ($\leq 3E_g$).[21] However, for NRs (and also seeded NRs), it is practically impossible to generate all possible singly excited states, even at relatively low excitation energies, due to the large DOS.[36] Therefore, in order to obtain the MEG efficiency, we propose a stochastic approach, where we sample the singly excited states and the corresponding MEG rates rather than calculating them all to perform the full summation formula for $n_{ex}(\omega)$. The approach can be summarized as follows:

(1) Calculate the single-particle DOS ($\rho(\varepsilon)$) using a stochastic trace formula.[30] Use convolutions to generate the density of single excited states ($\rho_X(E)$) and the negative/positive trion DOS ($\rho_T^-(\varepsilon)/\rho_T^+(\varepsilon)$).[30]

(2) Generate the negative/positive trion formation rates (eq 4) using the stochastic procedure.[30]

(3) Filter target electron and hole states with energies sampled from $\rho(\varepsilon)$ (above and below the Fermi energy, respectively), and for each electron–hole pair, calculate the transition dipole μ_{0S} at energy E_S.

(4) Use Γ_a^- and Γ_i^+ to generate the MEG rate for each electron–hole pair: $\Gamma_{S\equiv ia} = \Gamma_a^- + \Gamma_i^+$. Obtain $n_{ex}(\omega)$ by replacing the full summation expression (cf., eq 1) with an average over the sampled electron–hole pairs: $n_{ex}(\omega) = (1/N_S) \sum_S \mathcal{P}_S(\omega) \cdot [(2\Gamma_S + \gamma)/(\Gamma_S + \gamma)]$, where $\mathcal{P}_S(\omega) = \rho(\varepsilon_a)\rho(\varepsilon_i)P_S(\omega)$. The product $\rho(\varepsilon_a)\rho(\varepsilon_i)$ is used to correct for the density of electron and hole pairs at energy E_S. N_S is the number of excited states sampled at energy $E_S = \hbar\omega$, typically taken to be $N_S = 200$.

The first two steps have been developed previously by Baer and Rabani[30] and applied to both NCs and NRs.[30] The last two provide an extension to calculate the MEG efficiencies by sampling the singly excited states rather than calculating them all.

In Figure 1, we plot the negative and positive trion formations rates (upper panel, shown also in ref 30) and the MEG efficiency (lower panel, shown here for the first time) for a 3 nm diameter CdSe NC. The stochastic results are compared with the full summation approach, labeled "deterministic". The agreement between the stochastic and deterministic calculations is excellent, although the stochastic rates are slightly
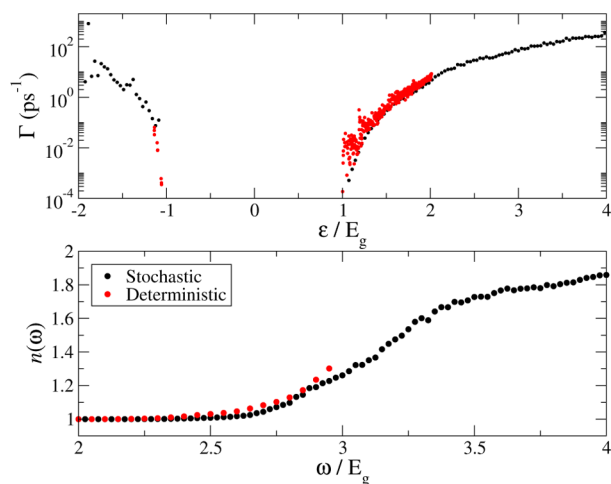
Figure 1. Trion formation rate (upper panel) and the MEG efficiency (lower panel) for a 3 nm diameter CdSe NC ($Cd_{232}Se_{251}$) as a function of scaled energy (ω is the photon energy, while ε is the energy of the electron (hole), for negative (positive) trions, measured from the bottom of the conduction (top of the valence) band). The full summation approach labeled "deterministic" is shown by red circles, and the stochastic approach spanning a larger energy range is shown by black circles.

underestimated compared with the average deterministic rates.[30] Comparing the results near the valence and conduction band edges, it is clear that the uniform sampling approach of the energy falls short in describing the trion formation rates for $\varepsilon/E_g \rightarrow \pm 1$. However, because these rates are very low compared to the phonon emission rate, γ, assuming a vanishing value does not affect the MEG efficiencies.

In the lower panel of Figure 1, we compare the stochastic MEG efficiencies to the deterministic approach. The stochastic approach slightly underestimates $n_{ex}(\omega)$, resulting from the small systematic deviation of the trion formation rates. However, the overall agreement is excellent, and the stochastic approach is reliable at energies much higher than those accessible by the deterministic calculations.

Moving on to the CdSe/CdS core/shell NRs of 20 nm length, we calculated the MEG formation rates and efficiencies for rod diameters D_{rod} of 4 and 6 nm and for several core

diameters D_{core} in the range of 2–4.5 nm in each case. The rods were faceted, and the center of the spherical CdSe core was placed at 1/3 of the length of the rod. The configurations of the seeded rods were relaxed using molecular dynamics runs for 100 ps at 300 K with a recently developed force field[44] accurately describing CdSe/CdS heterostructures.[45] The final configurations were quenched to remove structural effects of thermal fluctuations; thus, only one trajectory was used for each structure. The single-particle orbitals ($\psi_r(\mathbf{r})$) required for the calculation of the MEG rates were then generated for the relaxed configurations using semiempirical pseudopotential models on a real space grid,[46,47] with a Gaussian filtering function.[48]

In Figure 2, we show the MEG efficiencies (left panels) and the trion formation rates (right panels) for the two sets of rod diameters. The MEG efficiency increases with photon energy with an onset close to $3E_g$ and $3.5E_g$ for the $D_{rod} = 4$ and 6 nm, respectively. This is consistent with experiments for a wide range of confined nanostructures.[5] At energies above the onset energy, we find that the MEG efficiency at a scaled energy increases as the size of the NC seed decreases, consistent with calculations of spherical NCs.[21] For photon energies below the onset (between $2E_g$ and $3E_g$), the reverse is true, and the MEG efficiency is higher for larger seeds. This is depicted in the inset of Figure 2 and is qualitatively different from spherical NCs.

Despite the fact that the MEG efficiencies for energies between $2E_g$ and $3E_g$ are rather small in seeded NRs, understanding the origin of the behavior below the onset is still significant as it may prove useful in designing materials with higher MEG in this important range of energies. In the right panels of Figure 2, we plot the negative trion formation rate ($\Gamma_e^-(\varepsilon)$) for all corresponding cases. Because the MEG process is dominated by the formation of negative trions for CdSe NCs,[21] we focus on this channel and ignore, for the sake of the discussion (not in the calculations of the MEG efficiencies), the positive channel. For all cases studied, $\Gamma_e^-(\varepsilon)$ increases with the electron energy, similar to the behavior of spherical[29,32] and rod-shaped[36] nanostructures. However, there seems to be an isosbestic point about $\varepsilon/E_g = 1.75$ where $\Gamma_e^-(\varepsilon)$ changes behavior (this is more clearly observed in the DOTS discussed below). This isosbestic point is correlated with the crossover of the MEG efficiency with the NC seed size.
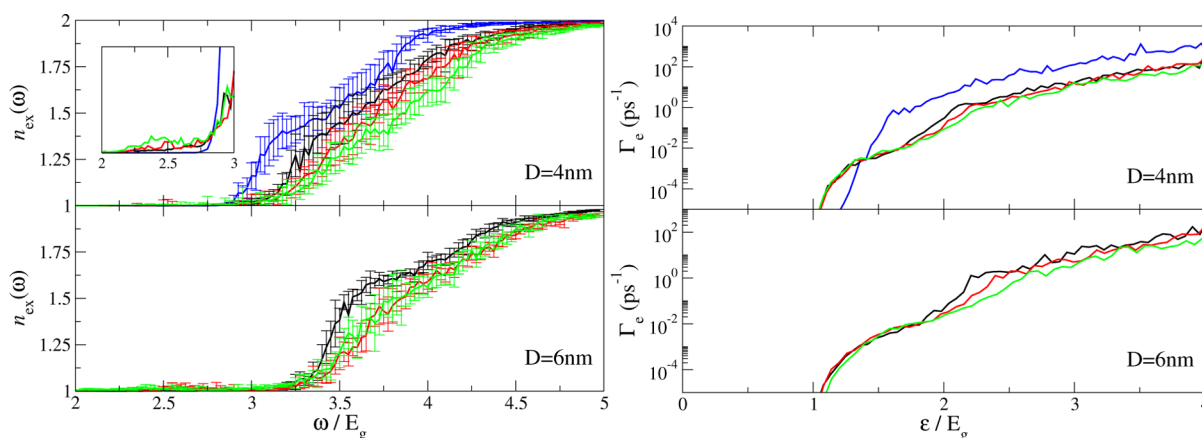

Figure 2. MEG efficiency for $D_{rod} = 4$ and 6 nm diameter NRs (upper and lower left panels, respectively) and the corresponding negative trion formation rates (right panels) for scaled energies. For the $D_{rod} = 4$ nm rods, the blue, black, red, and green curves represent seed sizes of $D_{core} = 0$, 2, 2.5, and 3 nm, respectively. For the $D_{rod} = 6$ nm rod, the black, red, and green curves represent seed sizes of $D_{core} = 2.5$, 3.5, and 4.5 nm, respectively. (Inset) Zoom in on the low-energy range.
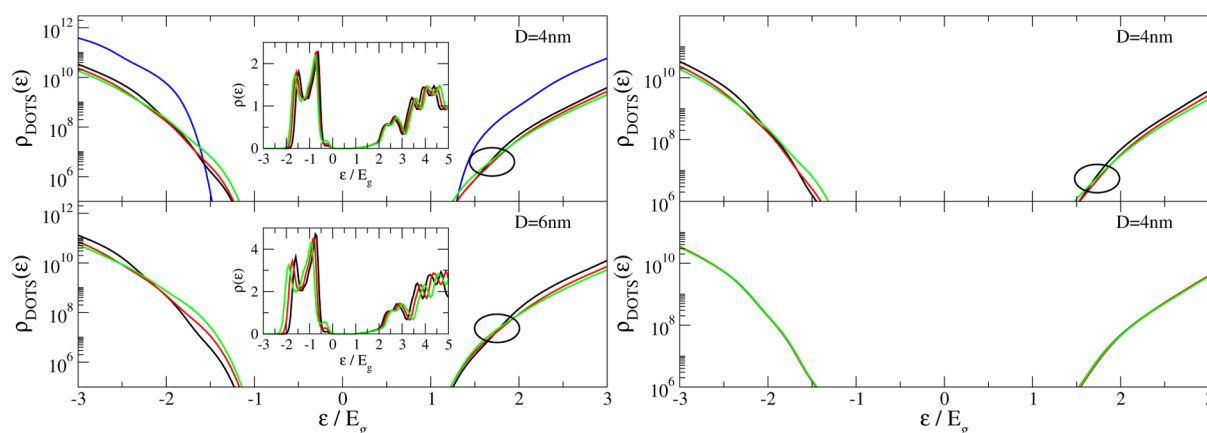
Figure 3. DOTS for D_{rod} = 4 and 6 nm NRs (upper and lower panels, respectively) and the artificial DOTS for a D_{rod} = 4 nm diameter (right panels) as described in the text. Insets show the corresponding DOS for each D_{rod}. For the D_{rod} = 4 nm rod, the blue, black, red, and green curves represent seed sizes of D_{core} = 0, 2, 2.5, and 3 nm, respectively. For the 6 nm rod, the black, red, and green curves represent seed sizes of D_{core} = 2.5, 3.5, and 4.5 nm, respectively.

To delineate the factors governing this behavior, we first note that the trion formation rates are given in terms of a product of the average square Coulomb coupling and the DOTS (cf., eq 4). The former shows a monotonic core-size dependence and a weak energy dependence (not shown).[30,36] Therefore, the isosbestic point must reflect a nonmonotonic behavior of the DOTS with D_{core}, which is indeed the case, as shown by the left panels of Figure 3. We find that both $\rho_T^-(\varepsilon)$ and $\rho_T^+(\varepsilon)$ exhibit an isosbestic point, while that for the negative DOTS (circled in black) is correlated with the isosbestic point of $\Gamma_e^-(\varepsilon)$.

Because the DOTS is given in terms of a triple convolution of the DOS, we also plot the DOS as insets to each panel in Figure 3. We focus on the energy regime about the Fermi energy (which is assumed at the top of the valence band and is set as the origin of the energy axis). Perhaps the most notable effect of the seed size on the DOS is the appearance of a shoulder near the valence band edge as D_{core} increases. This shoulder reflects the increasing DOS on the seed due to volume effects. In addition, the DOS shows a systematic shift in the position of the valence and conduction peaks resulting from small changes in the band gap as D_{core} increases (note that we scale the energy by the band gap E_g for each system). Here, the decrease of the band gap was mainly attributed to the change of the highest hole energy, which is localized on the seed.[47]

In the right panels of Figure 3, we plot the DOTS for two additional cases. The bottom panel assumes that the DOS of the holes for all seed sizes is identical; therefore, the observed change in the DOTS reflects the differences in the DOS of the electrons (i.e., the portion of the DOS above the Fermi energy). Clearly, all three sizes give the same DOTS. Therefore, one can conclude that the isosbestic point observed in the negative DOTS originates from the hole DOS (i.e., the portion of the DOS below the Fermi energy). The upper right panel of Figure 3 shows the DOTS for the case where the only difference in the DOS for the three values of D_{core} is assumed to be the aforementioned shoulder near the valence band edge. Clearly, this is sufficient to account for the isosbestic point. Thus, we conclude that the crossover behavior observed in the MEG efficiency can be attributed to the increase in the DOS near the valence band edge and at the same time the rather insignificant decrease in the band gap energy.

In conclusion, we have extended our stochastic approach to calculate the MEG efficiency in systems containing thousands of atoms within a master equation formalism. Rather than calculating all possible excitations and the corresponding MEG rates, we proposed to sample the electron−hole pairs and, for each pair, obtain the MEG rates (sum of the positive and negative trion formation rates) using our recently developed expeditious stochastic approach.[30] Application of the approach to quasi-type-II CdSe/CdS seeded NRs uncovered an interesting and unexpected behavior. Above the onset of MEG (around $3E_g$), the efficiency increases as D_{core} decreases, as expected. However, below this onset, the opposite is true, and larger seeds show higher MEG efficiencies, contrary to the situation in spherical NCs. This anomalous behavior was caused by the marked increase in DOS near the valence band edge as D_{core} dropped and the relative insensitivity of E_g to D_{core} (due to the quasi-type-II band alignment) .

Manipulating the DOS without affecting the band gap can be used to control MEG efficiencies in other semiconducting heterostructures. Of particular relevance are type-II NRs,[49] which are expected to yield larger MEG efficiencies, perhaps also due to the large internal fields across the interface between the two semiconducting materials.[33,34] These and other possible scenarios are currently under investigation.

■ **AUTHOR INFORMATION**

Corresponding Authors
*E-mail: hagai.eshet@gmail.com (H.E.)
*E-mail: roi.baer@huji.ac.il (R.B.)
*E-mail: dxn@chem.ucla.edu (D.N.)
*E-mail: eran.rabani@gmail.com (E.R.)

Notes
The authors declare no competing financial interest.

■ REFERENCES

(1) Beard, M. C.; Midgett, A. G.; Hanna, M. C.; Luther, J. M.; Hughes, B. K.; Nozik, A. J. Comparing Multiple Exciton Generation in Quantum Dots to Impact Ionization in Bulk Semiconductors: Implications for Enhancement of Solar Energy Conversion. *Nano Lett.* **2010**, *10*, 3019−3027.

(2) Klimov, V. I. Detailed-Balance Power Conversion Limits of Nanocrystal-Quantum-Dot Solar Cells in the Presence of Carrier Multiplication. *Appl. Phys. Lett.* **2006**, *89*, 123118.

(3) Christensen, O. Quantum Efficiency of Internal Photoelectric Effect in Silicon and Germanium. *J. Appl. Phys.* **1976**, *47*, 689−695.

(4) Kolodinski, S.; Werner, J. H.; Wittchen, T.; Queisser, H. J. Quantum Efficiencies Exceeding Unity Due to Impact Ionization in Silicon Solar-Cells. *Appl. Phys. Lett.* **1993**, *63*, 2405−2407.

(5) Padilha, L. A.; Stewart, J. T.; Sandberg, R. L.; Bae, W. K.; Koh, W.-K.; Pietryga, J. M.; Klimov, V. I. Carrier Multiplication in Semiconductor Nanocrystals: Influence of Size, Shape, and Composition. *Acc. Chem. Res.* **2013**, *46*, 1261−1269.

(6) Shabaev, A.; Hellberg, C. S.; Efros, A. L. Efficiency of Multiexciton Generation in Colloidal Nanostructures. *Acc. Chem. Res.* **2013**, *46*, 1242−1251.

(7) Schaller, R. D.; Klimov, V. I. High Efficiency Carrier Multiplication in PbSe Nanocrystals: Implications for Solar Energy Conversion. *Phys. Rev. Lett.* **2004**, *92*, 186601.

(8) Schaller, R. D.; Agranovich, V. M.; Klimov, V. I. High-Efficiency Carrier Multiplication through Direct Photogeneration of Multi-Excitons via Virtual Single-Exciton States. *Nat. Phys.* **2005**, *1*, 189−194.

(9) Ellingson, R. J.; Beard, M. C.; Johnson, J. C.; Yu, P. R.; Micic, O. I.; Nozik, A. J.; Shabaev, A.; Efros, A. L. Highly Efficient Multiple Exciton Generation in Colloidal PbSe and PbS Quantum Dots. *Nano Lett.* **2005**, *5*, 865−871.

(10) Schaller, R. D.; Petruska, M. A.; Klimov, V. I. Effect of Electronic Structure on Carrier Multiplication Efficiency: Comparative Study of PbSe and CdSe Nanocrystals. *Appl. Phys. Lett.* **2005**, *87*, 253102.

(11) Murphy, J. E.; Beard, M. C.; Norman, A. G.; Ahrenkiel, S. P.; Johnson, J. C.; Yu, P. R.; Micic, O. I.; Ellingson, R. J.; Nozik, A. J. PbTe Colloidal Nanocrystals: Synthesis, Characterization, and Multiple Exciton Generation. *J. Am. Chem. Soc.* **2006**, *128*, 3241−3247.

(12) Schaller, R. D.; Sykora, M.; Jeong, S.; Klimov, V. I. High-Efficiency Carrier Multiplication and Ultrafast Charge Separation in Semiconductor Nanocrystals Studied via Time-Resolved Photoluminescence. *J. Phys. Chem. B* **2006**, *110*, 25332−25338.

(13) Schaller, R. D.; Sykora, M.; Pietryga, J. M.; Klimov, V. I. Seven Excitons at a Cost of One: Redefining the Limits for Conversion Efficiency of Photons into Charge Carriers. *Nano Lett.* **2006**, *6*, 424−429.

(14) Beard, M. C.; Knutsen, K. P.; Yu, P. R.; Luther, J. M.; Song, Q.; Metzger, W. K.; Ellingson, R. J.; Nozik, A. J. Multiple Exciton Generation in Colloidal Silicon Nanocrystals. *Nano Lett.* **2007**, *7*, 2506−2512.

(15) Schaller, R. D.; Pietryga, J. M.; Klimov, V. I. Carrier Multiplication in InAs Nanocrystal Quantum Dots with an Onset Defined by the Energy Conservation Limit. *Nano Lett.* **2007**, *7*, 3469−3476.

(16) Trinh, M. T.; Polak, L.; Schins, J. M.; Houtepen, A. J.; Vaxenburg, R.; Maikov, G. I.; Grinbom, G.; Midgett, A. G.; Luther, J. M.; Beard, M. C.; et al. Anomalous Independence of Multiple Exciton Generation on Different Group IV−VI Quantum Dot Architectures. *Nano Lett.* **2011**, *11*, 1623−1629.

(17) Stewart, J. T.; Padilha, L. A.; Qazilbash, M. M.; Pietryga, J. M.; Midgett, A. G.; Luther, J. M.; Beard, M. C.; Nozik, A. J.; Klimov, V. I. Comparison of Carrier Multiplication Yields in PbS and PbSe Nanocrystals: The Role of Competing Energy-Loss Processes. *Nano Lett.* **2012**, *12*, 622−628.

(18) Franceschetti, A.; An, J. M.; Zunger, A. Impact Ionization Can Explain Carrier Multiplication in PbSe Quantum Dots. *Nano Lett.* **2006**, *6*, 2191−2195.

(19) Allan, G.; Delerue, C. Role of Impact Ionization in Multiple Exciton Generation in PbSe Nanocrystals. *Phys. Rev. B* **2006**, *73*, 205423.

(20) Shabaev, A.; Efros, A. L.; Nozik, A. J. Multiexciton Generation by a Single Photon in Nanocrystals. *Nano Lett.* **2006**, *6*, 2856−2863.

(21) Rabani, E.; Baer, R. Distribution of Multiexciton Generation Rates in CdSe and InAs Nanocrystals. *Nano Lett.* **2008**, *8*, 4488−4492.

(22) Isborn, C. M.; Kilina, S. V.; Li, X. S.; Prezhdo, O. V. Generation of Multiple Excitons in PbSe and CdSe Quantum Dots by Direct Photoexcitation: First-Principles Calculations on Small PbSe and CdSe Clusters. *J. Phys. Chem. C* **2008**, *112*, 18291−18294.

(23) Isborn, C. M.; Prezhdo, O. V. Charging Quenches Multiple Exciton Generation in Semiconductor Nanocrystals: First-Principles Calculations on Small PbSe Clusterse. *J. Phys. Chem. C* **2009**, *113*, 12617−12621.

(24) Delerue, C.; Allan, G.; Pijpers, J. J. H.; Bonn, M. Carrier Multiplication in Bulk and Nanocrystalline Semiconductors: Mechanism, Efficiency, and Interest for Solar Cells. *Phys. Rev. B* **2010**, *81*, 125306.

(25) Witzel, W. M.; Shabaev, A.; Hellberg, C. S.; Jacobs, V. L.; Efros, A. L. Quantum Simulation of Multiple-Exciton Generation in a Nanocrystal by a Single Photon. *Phys. Rev. Lett.* **2010**, *105*, 137401.

(26) Fischer, S. A.; Madrid, A. B.; Isborn, C. M.; Prezhdo, O. V. Multiple Exciton Generation in Small Si Clusters: A High-Level, Ab Initio Study. *J. Phys. Chem. Lett.* **2010**, *1*, 232−237.

(27) Piryatinski, A.; Velizhanin, K. A. An Exciton Scattering Model for Carrier Multiplication in Semiconductor Nanocrystals: Theory. *J. Chem. Phys.* **2010**, *133*, 084508.

(28) Allan, G.; Delerue, C. Optimization of Carrier Multiplication for More Effcient Solar Cells: The Case of Sn Quantum Dots. *ACS Nano* **2011**, *5*, 7318−7323.

(29) Lin, Z.; Franceschetti, A.; Lusk, M. T. Size Dependence of the Multiple Exciton Generation Rate in CdSe Quantum Dots. *ACS Nano* **2011**, *5*, 2503−2511.

(30) Baer, R.; Rabani, E. Expeditious Stochastic Calculation of Multiexciton Generation Rates in Semiconductor Nanocrystals. *Nano Lett.* **2012**, *12*, 2123−2128.

(31) Velizhanin, K. A.; Piryatinski, A. Numerical Analysis of Carrier Multiplication Mechanisms in Nanocrystalline and Bulk Forms of PbSe and PbS. *Phys. Rev. B* **2012**, *86*, 165319.

(32) Rabani, E.; Baer, R. Theory of Multiexciton Generation in Semiconductor Nanocrystals. *Chem. Phys. Lett.* **2010**, *496*, 227−235.

(33) Gabor, N. M.; Zhong, Z. H.; Bosnick, K.; Park, J.; McEuen, P. L. Extremely Efficient Multiple Electron−Hole Pair Generation in Carbon Nanotube Photodiodes. *Science* **2009**, *325*, 1367−1371.

(34) Baer, R.; Rabani, E. Can Impact Excitation Explain Efficient Carrier Multiplication in Carbon Nanotube Photodiodes? *Nano Lett.* **2010**, *10*, 3277−3282.

(35) Sandberg, R. L.; Padilha, L. A.; Qazilbash, M. M.; Bae, W. K.; Schaller, R. D.; Pietryga, J. M.; Stevens, M. J.; Baek, B.; Nam, S. W.; Klimov, V. I. Multiexciton Dynamics in Infrared-Emitting Colloidal Nanostructures Probed by a Superconducting Nanowire Single-Photon Detector. *ACS Nano* **2012**, *6*, 9532−9540.

(36) Baer, R.; Rabani, E. Communication: Biexciton Generation Rates in CdSe Nanorods Are Length Independent. *J. Chem. Phys.* **2013**, *138*, 051102.

(37) Padilha, L. A.; Stewart, J. T.; Sandberg, R. L.; Bae, W. K.; Koh, W.-K.; Pietryga, J. M.; Klimov, V. I. Aspect Ratio Dependence of Auger Recombination and Carrier Multiplication in PbSe Nanorods. *Nano Lett.* **2013**, *13*, 1092−1099.

(38) Karki, K. J.; Ma, F.; Zheng, K.; Zidek, K.; Mousa, A.; Abdellah, M. A.; Messing, M. E.; Wallenberg, L. R.; Yartsev, A.; Pullerits, T. Multiple Exciton Generation in Nanocrystals Revisited: Consistent Calculation of the Yield Based on Pump−Probe Spectroscopy. *Sci. Rep.* **2013**, *3*, 2287.

(39) Klimov, V. I. Multicarrier Interactions in Semiconductor Nanocrystals in Relation to the Phenomena of Auger Recombination and Carrier Multiplication. *Annu. Rev. Condens. Mater. Phys.* **2014**, *5*, 285−316.

(40) Prezhdo, O. V. Multiple Excitons and the Electron−Phonon Bottleneck in Semiconductor Quantum Dots: An Ab Initio Perspective. *Chem. Phys. Lett.* **2008**, *460*, 1−9.

(41) Chen, L. L.; Bao, H.; Tan, T. Z.; Prezhdo, O. V.; Ruan, X. L. Shape and Temperature Dependence of Hot Carrier Relaxation Dynamics in Spherical and Elongated CdSe Quantum Dots. *J. Phys. Chem. C* **2011**, *115*, 11400−11406.

(42) Carbone, L.; Nobile, C.; De Giorgi, M.; Sala, F. D.; Morello, G.; Pompa, P.; Hytch, M.; Snoeck, E.; Fiore, A.; Franchini, I. R.; et al. Synthesis and Micrometer-Scale Assembly of Colloidal CdSe/CdS Nanorods Prepared by a Seeded Growth Approach. *Nano Lett.* **2007**, *7*, 2942−2950.

(43) Li, H.; Kanaras, A. G.; Manna, L. Colloidal Branched Semiconductor Nanocrystals: State of the Art and Perspectives. *Acc. Chem. Res.* **2013**, *46*, 1387−1396.

(44) Grünwald, M.; Zayak, A.; Neaton, J. B.; Geissler, P. L.; Rabani, E. Transferable Pair-Potentials for CdS and ZnS Crystals. *J. Chem. Phys.* **2012**, *136*, 234111.

(45) Grünwald, M.; Lutker, K.; Alivisatos, A. P.; Rabani, E.; Geissler, P. L. Metastability in Pressure-Induced Structural Transformations of CdSe/ZnS Core/Shell Nanocrystals. *Nano Lett.* **2013**, *13*, 1367−1372.

(46) Rabani, E.; Hetenyi, B.; Berne, B. J.; Brus, L. E. Electronic Properties of CdSe Nanocrystals in the Absence and Presence of a Dielectric Medium. *J. Chem. Phys.* **1999**, *110*, 5355.

(47) Eshet, H.; Grunwald, M.; Rabani, E. The Electronic Structure of CdSe/CdS Core/Shell Seeded Nanorods: Type-I or Quasi-Type-II? *Nano Lett.* **2013**, *13*, 5880−5885.

(48) Neuhauser, D. Bound-State Eigenfunctions from Wave-Packets — Time-Energy Resolution. *J. Chem. Phys.* **1990**, *93*, 2611−2616.

(49) Luther, J. M.; Zheng, H.; Sadtler, B.; Alivisatos, A. P. Synthesis of PbS Nanorods and Other Ionic Nanocrystals of Complex Morphology by Sequential Cation Exchange Reactions. *J. Am. Chem. Soc.* **2009**, *131*, 16851−16857.